Journal of Solid State Chemistry 185 (2012) 101–106

Contents lists available at SciVerse ScienceDirect

Journal of Solid State Chemistry

journal homepage: www.elsevier.com/locate/jssc

Ternary lanthanum sulfide selenides α-$LaS_{2-x}Se_x$ ($0<x<2$) with mixed dichalcogenide anions X_2^{2-} (X=S, Se)

Christian Bartsch, Thomas Doert*

Department of Chemistry and Food Chemistry, Technische Universität Dresden, D-01062 Dresden, Germany

ARTICLE INFO

Article history:
Received 25 July 2011
Received in revised form
19 October 2011
Accepted 24 October 2011
Available online 10 November 2011

Keywords:
Polychalcogenides
Rare earth metal
Crystal structure
Raman spectra

ABSTRACT

Mixed lanthanum sulfide selenides $LaS_{2-x}Se_x$ ($0<x<2$) were obtained by metathesis reactions starting from anhydrous lanthanum chloride and alkali metal polychalcogenides. The $LaS_{2-x}Se_x$ compounds crystallize in space group $P2_1/a$, no. 14, and adopt the α-LnS_2 (Ln=Y, La–Lu) structure type with a pronounced site preference for the chalcogen atoms. The mixed chalcogenides form a complete miscible series with lattice parameters a=820–849 pm, b=413–425 pm and c=822–857 pm ($\beta\approx90^\circ$) following Vegard's rule. Raman signals indicate the presence of mixed X_2^{2-} dianions, a species rarely evidenced in literature, besides the well known anions S_2^{2-} and Se_2^{2-}. The band gaps of the $LaS_{2-x}Se_x$ compounds, determined by optical spectroscopy, decrease nearly linearly with increasing amount of selenium.

1. Introduction

Rare earth polychalcogenides $LnX_{2-\delta}$ (Ln=Y, La–Lu, X=S, Se, Te; $\delta\leq0.3$) are in the focus of scientists for decades because of their interesting structural, optical and electrical properties. They are, e. g., discussed for applications as far-infrared transmitting materials, lasers, phosphors, scintillators, and magneto-optical devices [1]. The optical and electrical properties vary with the constituting elements as well as with the chalcogen deficiency δ [2–4]. All binary polysulfides and polyselenides of trivalent rare earth metals investigated so far are semiconductors [3,4].

Detailed structure investigations revealed that the aforementioned polychalcogenides crystallize in superstructures of the tetragonal ZrSSi type (space group $P4/nmm$, $a\approx400$ pm, $b\approx400$ pm, $c\approx800$ pm). The non-deficient disulfides LnS_2 and diselenides $LnSe_2$ either adopt a twofold superstructure, the monoclinic α-LnS_2 – sometimes also called $CeSe_2$ type – ($P2_1/a$, $a\approx800$ pm, $b\approx400$ pm, $c\approx800$ pm, $\beta\approx90^\circ$) or the orthorhombic β-LaS_2 type ($Pnma$, $a\approx800$ pm, $b\approx1600$ pm, $c\approx400$ pm).[1] Different other kinds of superstructures are formed for compounds $LnX_{2-\delta}$ with $0<\delta\leq0.3$ due to the ordering of vacancies in the chalcogen layers [4c–e].

We were interested in investigating mixed polychalcogenides of the trivalent rare earth metals in order to check if a fine-tuning of the optical and electronic properties can be achieved in substitution series. The results for the compounds of the ternary lanthanum dichalcogenide series $LaS_{2-x}Se_x$ ($0<x<2$) are presented in the following.

2. Experimental

2.1. Synthesis

All manipulations with the starting reagents were carried out under purified argon (Air Liquide, 99.999%). Similar to binary rare earth metal disulfides [5], the ternary $LaS_{2-x}Se_x$ compounds ($0<x<2$) can be obtained by metathesis reactions of adequate amounts of anhydrous lanthanum chloride ($LaCl_3$: 99.9% Strem Chemicals GmbH, Kehl, Germany) and the alkaline metal polychalcogenides Na_2S_2 and K_2Se_3 according to the following reaction scheme:

$$LaCl_3+(1.5-0.75x)Na_2S_2+(0.75x)K_2Se_3 \rightarrow LaS_{2-x}Se_x+3Na_{(1-0.5x)}K_{0.5x}Cl+(1-0.5x)S+1.25xSe.$$

K_2Se_3 has been prepared by reaction of stoichiometric amounts of potassium (ingot, 99.99%, Chempur, Karlsruhe, Germany) with selenium in liquid ammonia at 210 K; Na_2S_2 was obtained by reaction of sodium (99.9%, Fluka), H_2S (99.9%, Messer-Griesheim) and sulfur in ethanol (99%, Merck; dried with sodium and diethyl terephthalate prior to use). The reaction mixtures were filled in glassy carbon crucibles which were loaded

* Corresponding author. Fax: +49 351 463 37287.
E-mail address: thomas.doert@chemie.tu-dresden.de (T. Doert).

[1] β-LaS_2 is a stacking variant of the α-LnS_2 type and not a superstructure of ZrSSi in the strict sense of group theory, i.e. there is no group-subgroup relation between the structures of ZrSSi and β-LnS_2.

0022-4596/$ - see front matter © 2011 Elsevier Inc. All rights reserved.
doi:10.1016/j.jssc.2011.10.039

in silica ampoules. The ampoules were flame sealed and placed in a chamber furnace which was then heated up to 850 °C with a heating ratio of 2 K/min. After one week the samples were cooled down to room temperature and rinsed with a 1:1 mixture of ethanol and water. The products consist of plate-like, lustrous crystals which show a red to black coloring in accordance with the respective selenium amount. Mixed lanthanum sulfide selenides can also be obtained by flux reactions starting from the elements in alkaline metal halides, like NaCl, using the same temperature program. Following both reaction routes, a slight excess of the respective chalcogenides is beneficial in order to avoid the formation of chalcogen deficient phases, above all $LnX_{1.9}$. Red selenium which is formed as one by-product dissolves in the ethanol/water mixture and can thus be easily removed from the target product. Sulfur, the other by-product, is not visible in optical microscopy and in X-ray powder diagrams. It probably deposits amorphously upon cooling the reaction mixtures and is rinsed off during the lavation process of the products.

2.2. Phase analyses

Phase purity of the reaction products was checked by X-ray powder diffraction (Panalytical, X'Pert PRO, Cu$K\alpha_1$ radiation, Bragg-Brentano setup). Using silicon as internal standard and the *LeBail* method [6] the lattice parameters of all single phase samples were determined by profile fitting with the program Jana2006 [7].

2.3. Chemical analyses

The sulfur and selenium contents of selected single phase samples were independently determined via ICP-OES analysis. Approximately 10 mg of the substances were molten into 0.7 mm capillaries, which were cracked in an autoclave with polytetrafluoroethylene (PTFE) inlay and digested using a 4 M HNO_3/HCl solution. The standard reference solutions for the rare-earth metals and sulfur were taken from Johnson Matthey.

2.4. Single crystal structure determination

Complete X-ray data sets of suitable crystals were recorded on image plate diffractometers (IPDS 1 or IPDS 2, Stoe & Cie., Darmstadt, Germany) at ambient temperature. LP corrections were performed with the program X-Red32 [8]. Numerical absorption corrections were applied using the refined crystal shape [8,9]. One data set was collected on a Bruker Apex2 CCD diffractometer, again at ambient temperature. LP corrections were performed with the Apex Suite software [10] and a multi-scan absorption correction was applied in this case [11]. Structure refinements were performed with Shelx-97 [12] or Jana2006 program packages [7]. The occupancy factors of the mixed occupied chalcogen positions *X*1 and *X*2 were coupled to 1 as no indications for deficiencies were obtained from chemical analyses. Further crystallographic information can be obtained from the FIZ-Karlsruhe (http://www.fiz-karlsruhe.de/obtaining_crystal_structure_data.html) on quoting the depository numbers stated in Table 2. As for the binary α-LnS_2 and $LnSe_2$ compounds, all investigated crystals of the mixed series were found to be twinned [4a,5b,13].

2.5. Optical spectroscopy

Raman spectra were recorded on single crystals with a Renishaw RM 2000 Raman microscope equipped with a 633 nm He/Ne Laser in the range from 100 nm to 500 nm.

The optical band gaps were determined by UV/Vis spectroscopy with a Varian Cary 4000 on powdered samples using $BaSO_4$ (Merck, white standard DIN 5033) as standard. Measurements were performed in the range from 350 nm to 900 nm with a Varian Praying Mantis device for diffuse reflectometry. The band gap was determined as the onset-wave-length at the absorption edge.

2.6. Electron microscopy

Transmission electron microscopy (TEM) and electron diffraction investigations were performed using a FEI Tecnai 10 electron microscope (FEI company, Eindhoven, The Netherlands) with a LaB_6-source at 100 kV acceleration voltage and at a camera length of 380 mm. Images were recorded with a Tietz slow scan CCD F224HD TVIPS camera ($2k \times 2k$ pixels, pixel size 24 μm, digitization 16 bit) with an active area of 49 mm × 49 mm (Tietz Video and Image Processing Systems GmbH, Gauting, Germany). The analyses of the TEM images were realized by means of the Digital Micrograph software (Gatan, USA).

3. Results and discussion

3.1. Phase analyses

According to the powder X-ray data, single phase samples were obtained from the metathesis reactions. The refined lattice parameters increase with increasing amount of selenium in accordance to Vegard's rule, Fig. 1. Despite the observed site preference of the chalcogen atoms (*vide infra*) no hints for the formation of an ordered superstructure, at the composition LaSSe, e. g., are observed in X-ray and TEM investigations (cf. Supplementary information).

3.2. Chemical analyses

The results of the chemical analyses via ICP-OES are in reasonable agreement with the initial element ratios as well as with the results from structure refinement on single crystal data, cf. Table 1.

3.3. Crystal structure

The mixed lanthanum sulfide selenides $LaS_{2-x}Se_x$ ($0 < x < 2$) crystallize in the α-LnS_2 (or $CeSe_2$) structure type in space group $P2_1/a$ (no. 14; non-standard setting of $P2_1/c$) which is adopted by the majority of the binary disulfides and all known diselenides of the trivalent rare earth metals [4,13]. The structure can be described as a twofold superstructure of the aristotype ZrSSi by

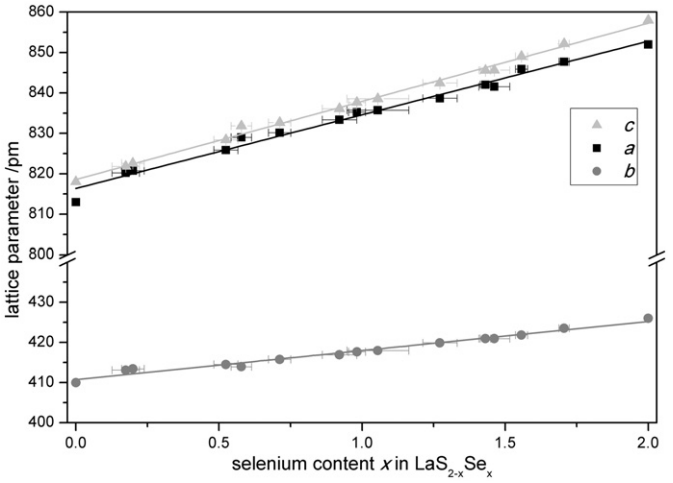

Fig. 1. Vegard plot of the lattice parameters of the $LaS_{2-x}Se_x$ samples.

following a three stepped symmetry reduction from $P4/nmm$ to $P2_1/a$ [13d]. The results of the structure analyses are briefly summarized in Table 2 and the atomic site parameters are given in Table 3 for $LaS_{1.47(1)}Se_{0.53(1)}$ as one example. As already stated, no indications for the formation of a superstructure were observed from the experimental data.

According to these refinements, the structure can be described as an alternating stacking of a puckered double slab of the composition $[LaX]^+$ and a planar polychalcogenide layer, consisting of a herringbone type pattern of dichalcogenide anions X_2^{2-}, Fig. 2. The structural formula can be written as $([LaX]^+)_2\,[X_2^{2-}]$. Accordingly, two crystallographically independent chalcogen sites are found: at $z \approx 0.63$ for the $X1$ atoms of the double slab and at $z \approx 0$ for the $X2$ atoms of the planar layer. Assuming mixed occupied positions for $X1$ and $X2$ and the usual constrains for site and displacement parameters and a coupling of the site occupancy factors $s.o.f.(Se) = 1 - s.o.f.(S)$ the refinements proceed smoothly to the results stated in Table 2.

The metal ions in this structure are surrounded by four $X2$ chalcogen atoms of the puckered double slab and four $X1$ chalcogen atoms of three different X_2^{2-} anions in a capped slightly distorted square antiprism. As expected, the average Ln–$X1$, the Ln–$X2$ and the $X2$–$X2$ distances increase with increasing Se amount of the compound. However, the average distances Ln–$X1$ are slightly shorter than the Ln–$X2$ distances. In the investigated series of mixed lanthanum sulfide selenides $LaS_{2-x}Se_x$, these two different chalcogen positions are mixed occupied by sulfur and selenium with a pronounced site preference. In accordance to its higher electrophilic behavior the sulfur atoms favor the $X1$ position which is closer to the lanthanum site. In contrast the $X2$ positions in the planar layer are favored by the selenium atoms. Due to this preferential occupation a characteristic elemental distribution across the whole range of the solid solution is observed, Fig. 3. However, in a complete miscible series without rigorous S/Se ordering, mixed $(S_{1-y}Se_y)_2^{2-}$ dianions with $0 < y < 1$ should occur. The increasing $X2$–$X2$ distances with increasing Se amount of the compounds can be taken as one hint for these mixed dianions, cf. Fig. 4.

Considering the quite different sizes of sulfur and selenium, the question arises, if a structure model with two distinct positions for S

Table 1
Chalcogen amounts of selected compounds as determined by X-ray structure refinement and ICP-OES.

Starting composition	Sulfur amount		Selenium amount	
	X-ray	ICP-OES	X-ray	ICP-OES
$LaS_{1.5}Se_{0.5}$	1.47(1)	1.47(2)	0.53(1)	0.56(1)
$LaS_{1.4}Se_{0.6}$	1.42(1)	1.38(4)	0.58(1)	0.62(1)
$LaS_{1.3}Se_{0.7}$	1.29(1)	1.26(1)	0.71(1)	0.74(1)
$LaS_{1.2}Se_{0.8}$	1.08(2)	1.13(1)	0.92(2)	0.93(1)
LaSSe	0.94(4)	0.98(2)	1.06(4)	1.03(2)
$LaS_{0.6}Se_{1.4}$	0.73(2)	0.75(2)	1.27(2)	1.28(3)
$LaS_{0.2}Se_{1.8}$	0.29(1)	0.28(1)	1.71(1)	1.72[a]

[a] Se amount re-calculated according to $x(Se) = 2 - x(S)$.

Table 2
Crystallographic data of mixed lanthanum sulfide selenides α-$LaS_{2-x}Se_x$ ($0 \le x \le 2$).

Compound	CSD-no.	Lattice parameters				Density/gcm^{-3}	Unique reflections/ parameters	Residual factors/%				Goodness of fit	Resid. el. density /e$^-$ × 10^{-6} pm^3	
								of averaging		for all data				
		a/pm	*b*/pm	*c*/pm	*β*/°			R_σ	R_{int}	R_1	wR_2		Min.	Max.
$LaS_{1.83}Se_{0.17}$	423,307	820.23(2)	413.12(1)	821.82(1)	90.05(1)	5.04	704/32	3.48	5.32	3.00	8.38	2.31	−1.31	0.96
$LaS_{1.80}Se_{0.20}$	423,308	820.76(1)	413.44(1)	822.59(1)	90.06(1)	5.05	1209/32	5.25	8.84	4.35	6.82	1.24	−2.77	2.97
$LaS_{1.47}Se_{0.53}$	423,309	825.85(1)	414.52(1)	828.40(1)	90.06(1)	5.33	477/32	1.11	5.43	2.18	5.11	1.18	−0.61	0.47
$LaS_{1.42}Se_{0.58}$	423,310	829.00(6)	413.97(3)	831.84(6)	90.22(1)	5.35	478/30	1.50	2.33	2.31	3.55	1.45	−1.00	1.00
$LaS_{1.29}Se_{0.71}$	423,311	830.16(2)	415.79(1)	832.67(7)	90.08(1)	5.46	531/32	1.71	2.51	1.93	4.33	1.12	−0.90	0.73
$LaS_{1.08}Se_{0.92}$	423,312	833.37(2)	416.91(2)	836.10(1)	90.13(1)	5.63	536/32	3.60	4.57	3.95	5.30	1.20	−1.58	1.52
$LaS_{1.02}Se_{0.98}$	423,313	835.24(2)	417.67(1)	837.64(1)	90.13(1)	5.66	1249/32	4.47	6.84	4.19	5.89	1.31	−2.18	2.39
$LaS_{0.94}Se_{1.06}$	423,314	835.72(2)	417.99(2)	838.55(2)	90.12(1)	5.73	373/30	4.44	5.96	4.59	7.29	1.14	−1.57	1.19
$LaS_{0.73}Se_{1.27}$	423,315	838.68(2)	419.90(1)	842.44(1)	90.21(1)	5.88	1071/34	1.22	7.36	3.51	8.12	2.55	−1.88	1.54
$LaS_{0.57}Se_{1.43}$	423,316	842.01(2)	420.70(1)	845.55(1)	90.14(1)	5.99	1437/32	3.61	5.66	4.26	5.38	1.12	−1.60	1.66
$LaS_{0.54}Se_{1.46}$	423,317	841.60(7)	420.98(4)	845.65(2)	90.14(1)	6.02	1673/34	1.74	4.93	4.06	7.95	2.41	−4.76	2.00
$LaS_{0.44}Se_{1.56}$	423,318	845.91(6)	421.85(2)	849.02(2)	90.29(1)	6.05	623/31	4.00	7.59	3.34	5.64	1.18	−2.35	1.13
$LaS_{0.37}Se_{1.63}$[a]	423,319	844.5(2)	422.25(6)	848.0(2)	90.06(1)	6.14	1332/34	1.16	9.21	4.51	9.04	3.05	−3.20	2.81
$LaS_{0.29}Se_{1.71}$	423,320	847.70(3)	423.53(1)	852.17(1)	90.15(1)	6.14	1151/32	2.27	3.00	2.44	5.11	1.09	−1.70	1.14
$LaS_{0.23}Se_{1.77}$[a]	423,321	846.12(3)	423.46(1)	852.27(3)	90.10(1)	6.22	1897/31	2.92	2.93	2.92	4.09	0.94	−1.08	1.32
$LaS_{0.21}Se_{1.79}$[a]	423,322	845.3(2)	424.23(7)	852.9(2)	90.24(2)	6.23	928/32	1.43	2.92	4.07	6.30	1.90	−0.98	1.06
$LaS_{0.14}Se_{1.86}$[a]	423,323	849.4(3)	425.1(2)	852.3(3)	90.03(3)	6.26	859/33	1.27	4.19	3.39	6.72	2.20	−2.74	2.24
$LaS_{0.08}Se_{1.92}$[a]	423,324	848.7(1)	424.78(5)	857.2(2)	90.04(1)	6.30	661/31	3.75	5.48	3.74	7.61	1.08	−1.40	1.47

[a] Lattice parameters from single crystal refinement.

Table 3
Site, occupancy and displacement parameters (10^4 pm^2) for $LaS_{1.47(1)}Se_{0.53(1)}$ as an example; structure model with mixed S/Se positions.

Atom	*site*	*x*	*y*	*z*	*occ.*	U_{11}	U_{22}	U_{33}
La1	4*e*	0.1285(1)	0.2151(1)	0.2802(1)	1	69(3)	77(3)	93(3)
S1	4*e*	0.1249(4)	0.2398(4)	0.6351(2)	0.945(8)	67(10)	74(10)	88(10)
Se1	4*e*	0.1249(4)	0.2398(4)	0.6351(2)	0.055(8)	67(10)	74(10)	88(10)
S2	4*e*	0.3865(2)	0.1704(3)	0.9979(2)	0.529(9)	97(7)	120(8)	78(5)
Se2	4*e*	0.3865(2)	0.1704(3)	0.9979(2)	0.471(9)	97(7)	120(8)	78(5)

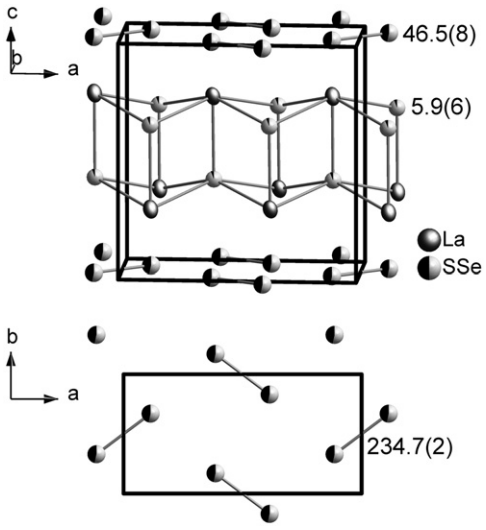

Fig. 2. Crystal structure of $LaS_{1.47(1)}Se_{0.53(1)}$, the Se amount of the mixed occupied positions is given in the upper panel, the distances in the dianion in the lower panel; atoms are shown on a 99% probability level.

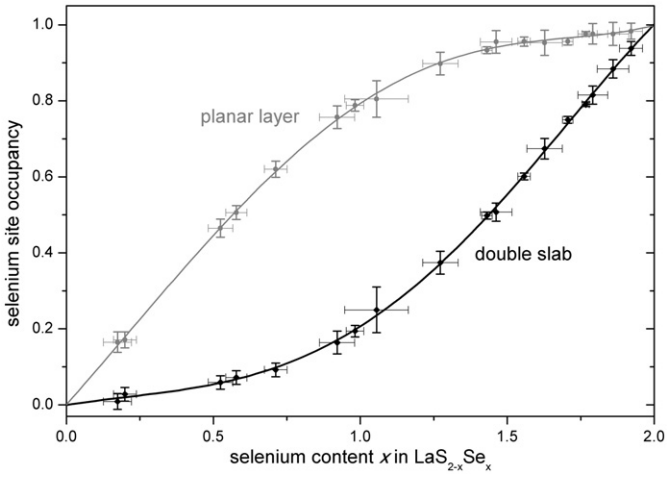

Fig. 3. Occupation of the two different chalcogen positions as function of the selenium content.

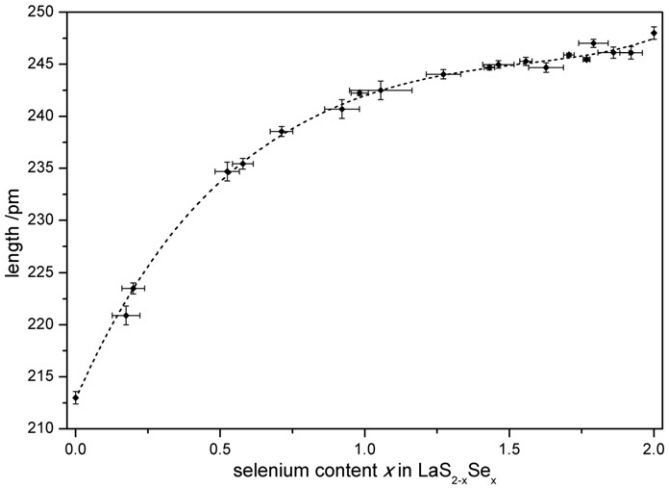

Fig. 4. Interatomic distances within the dichalcogenide anions X_2^{2-} as function of the selenium content.

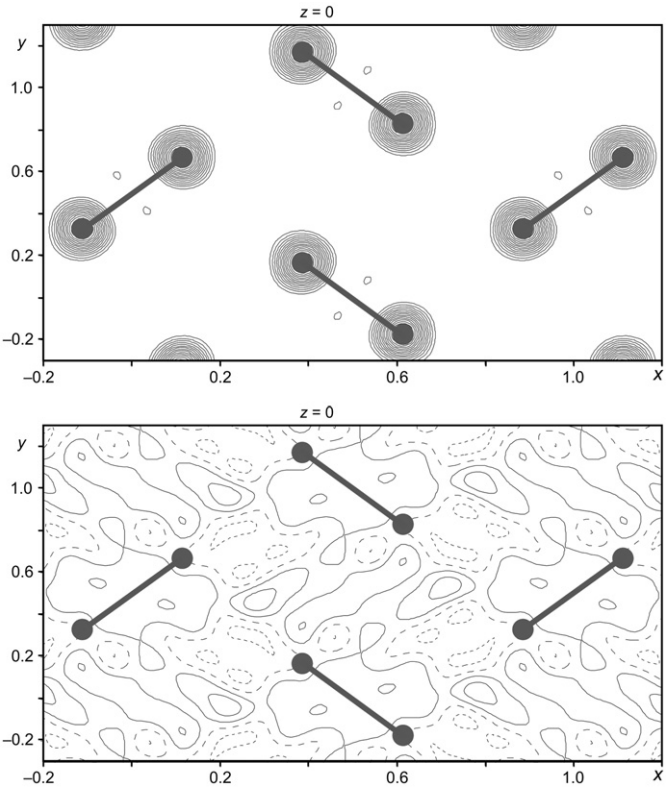

Fig. 5. *Fourier* map (F_{obs}, top, contour lines in steps of $5e^-/10^6pm^3$) and *Fourier* difference map (F_{obs}–F_{calc}, bottom, contour lines in steps of $0.2e^-/10^6pm^3$) for $LaS_{1.47(1)}Se_{0.53(1)}$ for $z=0$, negative values are indicated by dashed lines.

and Se in the puckered double slab and/or in the planar layer can be refined. There is no any evidence for an ordering into S_2^{2-} and Se_2^{2-} anions, e.g., from the respective *Fourier* and *Fourier* difference maps as can be seen in Fig. 5 for $LaS_{1.47(1)}Se_{0.53(1)}$ as an example. In some structure models, however, somewhat elongated displacement parameters may be taken as a hint for such an S/Se ordering. A free refinement of such a model with S/Se ordering is not possible as it suffers from large correlations, resulting in large standard deviations and physically meaningless displacement parameters, e.g. Nevertheless, such a model can be constructed and refined using constrained isotropic displacement parameters. In doing so, the residual values and the electron density hardly change (cf. Supplementary information for the example of $LaS_{1.47(1)}Se_{0.53(1)}$). The result for a calculation with distinct S and Se sites in the planar chalcogen layer is shown in Table 4 and Fig. 6 for the example of $LaS_{1.47(1)}Se_{0.53(1)}$ again.

The bond distances within the dichalcogenide anions are then computed to 215.3(17) pm for the disulfide, 243.0(8) pm for the diselenide and 229.1(13) pm for the mixed $(S_{1-y}Se_y)_2^{2-}$ dianions, respectively. Despite the large standard deviations, the bond distances for the homonuclear dianions are in good agreement with those found in binary disulfides and diselenides of the rare earth metals [4,13]. A sketch of a possible ordering pattern in the planar chalcogen layer is given in Fig. 6 (the number of S and Se atoms in the sketch do not match the calculated occupancies precisely).

3.4. Optical spectroscopy

Raman spectra were recorded to confirm of the existence of mixed dichalcogenide anions X_2^{2-}. As the respective Raman spectra of the binaries α-LaS_2 [3,14] and $LaSe_2$ [15] are well investigated, a detailed discussion can be skipped here, the respective data are taken as

references. The Raman signal for the Se–Se stretching mode of the Se_2^{2-}dianion at about 215 cm^{-1} can clearly be observed for samples with $x \geq 0.1$, Fig. 7. At 400 cm^{-1}, the doublet signal for the S–S stretching mode (S_2^{2-}dianions) is found for samples with $x \leq 1.7$. These wave numbers are in good agreement with literature data [3,14,15]. Between these two signals, an additional Raman signal is found only for the mixed chalcogenides ($0 < x < 2$) which can be attributed to the stretching mode of a mixed $(S_{1-y}Se_y)_2^{2-}$ dimer ($0 < y < 1$). The intensity of this signal is quite pronounced for low selenium contents. This is reasonable as the Raman intensity of a stretching mode mainly depends on its symmetry and on the polarizability of the atoms. A small amount of the more polarizable Se atoms in a sulfur-rich environment should thus yield comparatively high Raman intensities. Consequently, the intensity of this stretching mode decreases for higher amounts of Se and is zero in both binaries. Moreover, the S–Se stretching mode shows a clear wavelength shift in accordance to the selenium amount of the

Table 4
Site, occupancy and displacement parameters (10^4 pm^2) for $LaS_{1.47(1)}Se_{0.53(1)}$ as an example; structure model with distinct S and Se positions in the planar chalcogen layer.

Atom	*site*	*x*	*y*	*z*	*occ.*	U_{11}	U_{22}	U_{33}
La1	4*e*	0.1285(1)	0.2151(1)	0.2802(1)	1	67(3)	77(3)	91(3)
S1	4*e*	0.1250(5)	0.2398(4)	0.6349(2)	0.940(8)	70(10)	77(10)	84(9)
Se1	4*e*	0.1250(5)	0.2398(4)	0.6349(2)	0.060(8)	70(10)	77(10)	84(9)
S2	4*e*	0.392(2)	0.149(2)	0.998(1)	0.525(9)	81(6)[a]		
Se2	4*e*	0.3836(8)	0.1793(9)	0.9979(5)	0.475(9)	81(6)[a]		

[a] U_{iso} (isotropic refinement only).

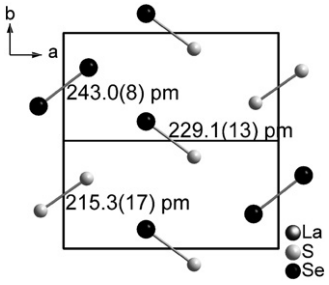

Fig. 6. Sketch of a possible ordering pattern in the planar chalcogen layer of $LaS_{1.47(1)}Se_{0.53(1)}$; atoms are shown on a 99% probability level.

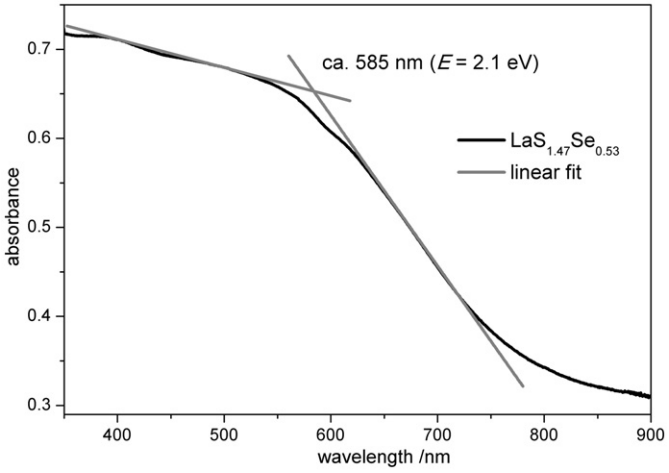

Fig. 8. Band gap determination of $LaS_{1.47(1)}Se_{0.53(1)}$ from UV/vis-spectra as example.

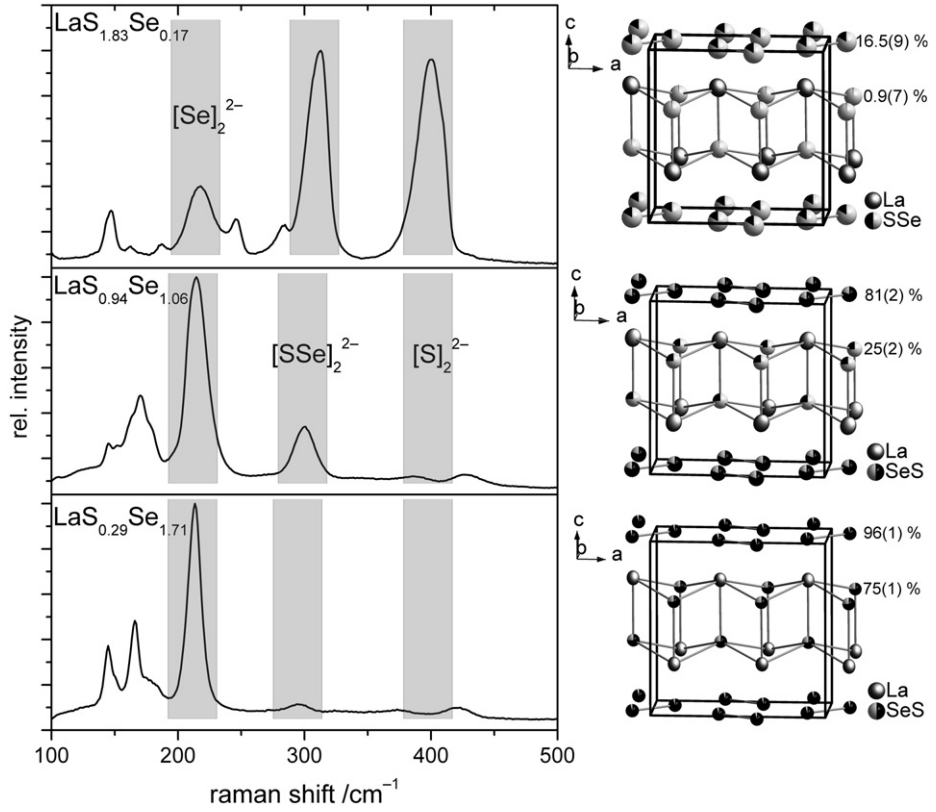

Fig. 7. Raman spectra of selected $LaS_{2-x}Se_x$ compounds; the ranges for the signals of the stretching modes of Se_2^{2-} at ≈ 215 cm^{-1}, $(S_{1-y}S_y)_2^{2-}$ at ≈ 300 cm^{-1} and S_2^{2-} at ≈ 400 cm^{-1} are highlighted.

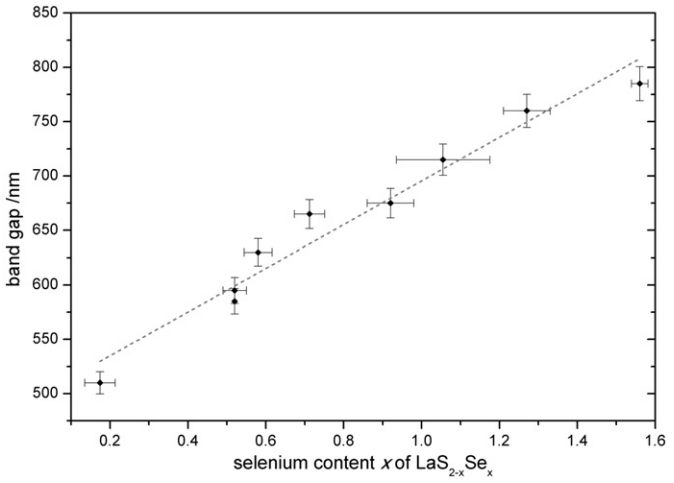

Fig. 9. Band gaps as a function of the selenium content.

sample. This signal is found at about 320 cm^{-1} for low Se contents and at ca. 290 cm^{-1} for higher Se amounts, Fig. 7. A similar behavior has been found in the pyrite type series $RuS_{1-x}Se_x$ [16], another rare example evidencing a $(S_{1-y}Se_y)_2^{2-}$ dianion in solid state bulk material.

Finally the optical band gaps of selected samples were determined by UV/vis spectroscopy, Fig. 8. The band gaps vary almost linearly with the selenium amount between 500 nm (2.48 eV for $LaS_{1.83}Se_{0.17}$) and 800 nm (1.55 eV for $LaS_{0.44}Se_{1.56}$). As can be expected, the band gaps decrease with increasing amount of selenium, Fig. 9.

4. Conclusions

A complete series of crystalline mixed lanthanum sulfide selenides $LaS_{2-x}Se_x$ $(0 \le x \le 2)$ was obtained via metathesis reaction. The compounds have been identified via powder and single crystal X-ray data and chemical analyses. The ternary compounds adopt the α-LnS_2 structure with a pronounced site preference of the two crystallographically independent chalcogen positions. The lattice parameters *a*, *b* and *c*, and hence the unit cell volumes, increase with the selenium content of the compounds according to Vegard's rule. On the other hand, the optical band gaps decrease with increasing selenium content. Raman measurements evidence a mixed $(S_{1-y}Se_y)_2^{2-}$ chalcogenide $(0 < y < 1)$ besides the well known S_2^{2-} and Se_2^{2-} species.

Acknowledgment

This work was financially supported by the *Deutsche Forschungsgemeinschaft* (DFG, Bonn Germany). We thank Ch. Ziegler, A. Klausch, and E. Ahrens (Department of Chemistry and Food Chemistry, TU Dresden) for Raman and UV/Vis measurements and for practical support, respectively. Special thanks to Dr. G. Auffermann and Dr. P. Simon (Max Planck Institute for Chemical Physics of Solids, Dresden) for chemical analyses and TEM investigations.

Appendix A. Supporting information

Supplementary data associated with this article can be found in the online version at doi:10.1016/j.jssc.2011.10.039.

References

[1] (a) P.N. Kumta, S.H. Risbud, J. Mater. Sci. 29 (1994) 1135;
(b) C. Witz, D. Huguenin, J. Lafait, S. Dupont, M.L. Theye, J. Appl. Phys. 79 (1996) 2038;
(c) R. Mauricot, J. Bullot, J. Wery, M. Evain, Mater. Res. Bull. 31 (1996) 263;
(d) A. Grzechnik, J. All., Comp 317 (2001) 190.
[2] (a) K. Stöwe, J. Solid State Chem. 149 (2000) 155;
(b) K. Stöwe, Z. Kristallogr. 216 (2001) 215;
(c) P. Böttcher, Th. Doert, H. Arnold, R. Tamazyan, Z. Kristallogr. 215 (2000) 246.
[3] (a) I.G. Vasilyeva, in: K.A. Gschneidner Jr., L. Eyring, G.H. Lander (Eds.), Handbook on the Physics and Chemistry of the Rare Earths, Vol. 32, Elsevier, Amsterdam, 2001, pp. 567–607 chapter 209 (Polysulfides);
(b) A. Grzechnik, Physica B 262 (1999) 426.
[4] (a) C.J. Müller, U. Schwarz, P. Schmidt, W. Schnelle, Th. Doert, Z. Anorg. Allg. Chem. 636 (2010) 947;
(b) Th. Doert, Chr. Graf, W. Schnelle, I.G. Vasilyeva, Inorg. Chem., submitted for publication;
(c) Th. Doert, Chr. Graf, P. Lauxmann, Th. Schleid, Z. Anorg. Allg. Chem. 633 (2007) 2719–2724;
(d) Th. Doert, E. Dashjav, B.P.T. Fokwa, Z. Anorg. Allg. Chem. 633 (2007) 261;
(e) Chr. Graf, Th. Doert, Z Kristallogr 224 (2009) 568–579.
[5] (a) John H. Chen, Peter K. Dorhout, J. Solid State Chem 117 (1995) 318–322b;
(b) Th. Schleid, P. Lauxmann, Chr. Graf, Chr. Bartsch, Th. Doert, Z. Naturforsch. 64b (2009) 189.
[6] A. LeBail, H. Duroy, J.L. Fourquet, Mater Res. Bull. 23 (1988) 447.
[7] JANA2006, Crystallographic Computing System, V. Petricek, M. Dusek, L. Palatinus, Prague, 2010.
[8] X-Red32, Program for data reduction and absorption correction, Stoe & Cie., Darmstadt, Germany, 1998.
[9] X-Shape, Crystal shape optimization, Stoe & Cie., Darmstadt, Germany, 1998.
[10] Apex Suite, Bruker-AXS, Madison, WI, USA, 2008.
[11] SADABS, G.M. Sheldrick, Bruker-AXS, Karlsruhe, Germany, 2002.
[12] G.M. Sheldrick, SHELX-97, Structure solution and refinement software, University of Göttingen, Germany, 1997.
[13] (a) S. Bénazeth, D. Carré, P. Laruelle, Acta Crystallogr. B38 (1982) 33;
(b) S. Bénazeth, D. Carré, P. Laruelle, Acta Crystallogr. B38 (1982) 37;
(c) R. Tamazyan, H. Arnold, V.N. Molchanov, G.M. Kuzmicheva, I.G. Vasilyeva, Z. Kristallogr. 215 (2000) 272;
(d) Th. Doert, Ch. Graf, Z. Anorg. Allg. Chem. 631 (2005) 1101;
(e) C.J. Müller, Th. Doert, U. Schwarz, Z. Kristallogr. 226 (2011) 646.
[14] (a) S. Bénazeth, M. Guittard, J. Flahaut, J. Solid State Chem. 37 (1981) 44;
(b) B. Le Rolland, P. McMillan, P. Colombet, C. R. Acad. Sci., Serie II 312 (1991) 217;
(c) B. LeRolland, P. Molinié, P. Colombet, P.F. McMillan, J. Solid State Chem. 113 (1994) 312.
[15] A. Grzechnik, J.Z. Zheng, D. Wright, W.T. Petuskey, P.F. Mcmillan, J. Phys. Chem. Solids 57 (1996) (1625).
[16] H.C. Lin, M.C. Lee, S.S. Lin, Y.S. Huang, Solid State Commun. 82 (1992) 821.